ACS Sustainable Chemistry & Engineering

Research Article

pubs.acs.org/journal/ascecg

Energy Modeling of Electrochemical Anodization Process of Titanium Dioxide Nanotubes

Bingbing Li,[†] Xianfeng Gao,[†] Hong-Chao Zhang,[‡] and Chris Yuan*[,†]

[†]Department of Mechanical Engineering, University of Wisconsin-Milwaukee, Milwaukee, Wisconsin 53211, United States

[‡]Department of Industrial Engineering, Texas Tech University, Lubbock, Texas 79409, United States

Supporting Information

ABSTRACT: Titanium dioxide nanotubes have some unique properties and have found a wide range of potential applications. Electrochemical anodization is a popular method for synthesis of TiO_2 nanotubes. While the TiO_2 nanotube morphologies are mainly controlled by the supplied electrical power and anodization time, energy inputs into the electrochemical anodization process also affect the sustainability performance of the technology in future industrial applications. This paper presents a mathematical modeling approach for understanding the direct energy consumptions in the electrochemical anodization process in which the process is divided into five stages including cleaning/drying, oxide layer formation, chemical diffusion, physical diffusion, and calcinations. Mathematical models based on thermodynamics and kinetics are developed for each of the above stages and validated using both experimental and literature data. The results demonstrate that about 67% of the energy input in the electrochemical anodization process is required by the physical diffusion. These models and analyses results could help understand the internal energy flow pattern within the electrochemical anodization process and aid sustainable development of the technology for future large-scale industrial applications.

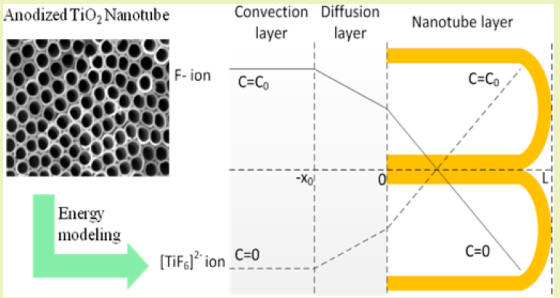

KEYWORDS: *Energy analysis, Thermodynamics, Kinetics, Electrochemical anodizing process, Titanium dioxide nanotubes, Sustainability improvement*

INTRODUCTION

Titanium dioxide nanotubes (TiO_2 NT) have attracted substantial interest in recent years due to their superior material properties.[1] The precisely oriented TiO_2 NT arrays possess an outstanding charge transport and carrier lifetime property that has found great potential in a broad array of industrial applications including photocatalysis for organic waste decomposition,[2] photoelectrolysis,[3] polymer-based bulk heterojunction photovoltaics,[4] biomedical applications,[5] gas sensing,[6] doping,[7] solar energy harvesting,[8,9] and energy storage devices.[10,11] Current methods for TiO_2 NT synthesis can be classified into two main categories based on the synthesis mechanism: template-assisted methods and nontemplate methods. In the template-assisted method, there are various routes to prepare TiO_2 NT including sol−gel transcription (wet-chemical technique) method,[12] atomic layer deposition (ALD),[13] chemical vapor deposition (CVD), electro deposition, photo deposition, thermosetting, and seeded growth.[14] Nontemplate TiO_2 NT synthesis procedures typically include the hydrothermal/solvothermal approach[15] and electrochemical anodizing process.[16] When compared, the nontemplate methods have better scale-up potential than the template-assisted methods because the nontemplate methods are simple and lower in cost to operate in real industrial-scale manufacturing. Among the three nontemplate methods, hydrothermal and solvothermal methods rely heavily on toxic chemicals to assist in the reactions to synthesize TiO_2 NTs.[17−19] But, toxic chemicals could have adverse impacts on human health and accordingly can lower the sustainability performance of the technology.[20] In comparison, electrochemical anodization is a process to synthesize TiO_2 NT via oxidation of a metallic titanium substrate in a mixed electrolyte typically composed of dionized water, ethylene glycol, and ammonium.[21] The electrochemical anodization process has a high potential in future industrial-scale productions due to its relatively low environmental impact, low cost, and fast oxidation process.

While currently most efforts have been made on the technology development and precise control of the TiO_2 NT morphologies, little attention has been paid to the sustainability performance of the TiO_2 NT synthesis process, and no energy modeling study has ever been conducted on the electrochemical anodization of TiO_2 NT. To understand and minimize the potential environmental impacts of the technology from energy perspectives, it is important to model and understand the energy requirements for the TiO_2 NT synthesis process in order to improve its energy efficiency and the overall sustainability performance. Compared with the bulk

Received: August 18, 2013
Revised: November 1, 2013
Published: December 1, 2013

TiO_2 manufacturing processes, nanoscale TiO_2 synthesis processes are usually much more energy intensive.[22] A previous study showed that NT fabrication could require 13−50 times more energy than traditional materials on an equal mass basis.[23] In electrochemical anodization, the TiO_2 NT morphologies are mainly controlled by the supplied power and the anodizing time.[10] As a result, accurate modeling and precise control of the energy inputs into the electrochemical anodization of the TiO_2 NT process are critical in sustainable development of the electrochemical anodization technology for future large-scale industrial applications.

For process energy modeling, thermodynamic analysis including energy and exergy analyses is an effective approach for understanding the energy flows and reducing exergy losses in the electrochemistry process. In principle, energy is never destroyed but always conserved based on the first law of thermodynamics.[24] Exergy is the maximum amount of useful work available in a process to equilibriate with the reference state and the quality of energy that provides a rigorous way of accounting for losses.[25] But TiO_2 nanomaterials are relatively new, and only a few research works have been published on some related sustainability studies. For example, Gottschalk formulated probabilistic material flow models to estimate environmental release of preparing TiO_2 NT from cradle to grave.[26] Grubb calculated environmental impact of emissions, energy requirements, and exergetic losses for TiO_2 nanoparticle production based on the altairnano hydrochloride process.[27] Theis et al. addressed the manufacturing energy requirement, embodied energy, material efficiency, and environmental properties of various nanomaterials including TiO_2 NT.[28] From the literature, the limited sustainability studies of TiO_2 nanomaterials were all conducted on macro-scale analysis, while only a few analyses on the process level of thermodynamic energy analysis were conducted. Also, no study was ever conducted on the direct energy analysis of the electrochemical anodization process of TiO_2 nanotubes.

In this paper, a numerical energy analysis of the electrochemical anodizing process for the TiO_2 NT synthesis is presented with mathematical models and validated results. The energy model is developed based on thermodynamics and kinetics for the electrochemical anodization of the TiO_2 NT synthesis, including process parameters, defined boundaries, and operating conditions. In the following sections, the experimental characterization, model development, and numerical analysis for the electrochemical anodizing process of TiO_2 NT are described in detail. The energy requirements for various stages of the synthesis process are quantified and benchmarked. The potential of the sustainability improvement is then discussed based on the energy analysis results. The created model is validated by the electrochemical anodizing process of TiO_2 NT, and the developed model can be extended to other similar nanomaterial synthesis processes in future.

METHODOLOGY

For fabricating TiO_2 nanotubes through electrochemical anodization, a Ti foil was first washed in ethanol to remove the surface impurities. The anodization was conducted within a two-electrode electrochemical cell using the Ti foil with a 0.25 mm thickness and 99.97% purity from ESPI as the anode, a platinum foil as cathode, and a fluoride ion based electrolyte. The electrolyte was 0.4 wt % ammonium fluoride (NH_4F 98%, Aldrich Corp.) and 5 wt % deionized water dissolved in ethylene glycol (99%, EMD Millipore). DC electricity is then supplied to the system with precise controlled power and time to perform the electrochemical anodization. Overall, the electrochemical anodization is a selective etching process in terms of a competition between several physical and chemical reactions including anodic oxide formation, chemical dissolution, and complexation. The key processes involved in the electrochemical anodization of TiO_2 nanotubes include the following three steps: (1) An oxide layer growth on the surface of the metal occurs due to interaction of the metal with oxygen ions. After the formation of an initial oxide layer, these anions migrate through the oxide layer reaching the metal/oxide interface where they react with the metal. Furthermore, an oxide layer grown is dominated by the migration of ions Ti^{4+} and O^{2-} in the growing compact layer. The compact anodically formed oxide layer is indicated in Figure 1a.

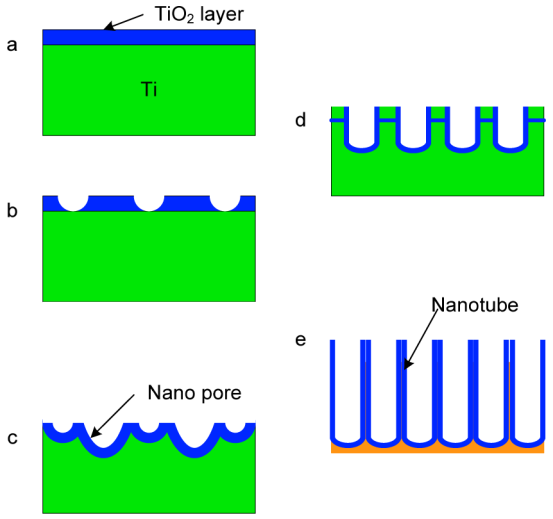

Figure 1. Schematic of the electrochemical anodizing process and anodic morphologies: (a) formation of oxide layer, (b) random growth of pores, (c) self-ordered oxides nanopores, (d) disorganized oxide NT formation, and (e) ordered nanotube.

(2) Field-assisted dissolution of the oxide occurs at the oxide/electrolyte interface. Because of the applied electric field, the Ti−O bond is subject to polarization and is weakened to facilitate dissolution of the metal cations. Ti^{4+} cations are dissolved into the electrolyte, and the free oxygen anions migrate toward the metal/oxide interface to interact with the metal. After the surface is locally activated and pores begin to grow randomly due to the initial localized dissolution of the oxide (Figure 1b), the barrier layer at the bottom of the pits becomes relatively thin and the electric field intensity increases across the remaining barrier layer, resulting in a further pore growth (Figure 1c). (3) Chemical dissolution of the oxide by the fluoride acidic electrolyte takes place during anodization. The formation of nanotube arrays is the result of the above three simultaneously occurring processes after the initial stage. Once the rate of TiO_2 formation is almost equal to the rate of TiF_6^{2-} formation and dissolution, the nanotubes will grow steadily as shown in Figure 1d. Finally the ordered nanoporous layers (Figure 1e) are obtained at an equilibrium state between the electrochemical etching rate and the chemical dissolution rate on the top surface of the nanotubes. On the basis of the description of the above synthesis and anodization process, the complete electrochemical anodization of the ordered TiO_2 NT is divided into five stages in order to model the required energy inputs and to understand the internal energy flow pattern of the technology from a process-based thermodynamic perspective: cleaning and drying, formation of oxide layer, chemical diffusion (related to field-assisted dissolution of oxide and chemical dissolution of oxide), physical diffusion (related to the diffusion of fluoride species to the tube bottom or the transport of reacted TiF_6^{2-} species), and calcinations.

In this section, specific process-based energy models are built for TiO_2 NT synthesis using the electrochemical anodization technique. For the electricity consumed in cleaning and drying, energy could be simply measured using a power meter based on the device operations.

During the formation of the oxidation layer, the major activity is the migration of ions Ti^{4+} and O^{2-} on the metal Ti surface, so the model is created based on chemical thermodynamics. After the formation of the oxidation layer, the anodization is dominated by chemical and physical diffusions. The energy model for chemical diffusion is created based on chemical thermodynamics, while electric current potential model for physical diffusion is created based on kinetics. At the end, an energy model for the calcination process of amorphous TiO_2 NT is also developed. Figure 2 illustrates the system boundary for this analysis, with Gibbs free energy associated with each process provided in the figure.

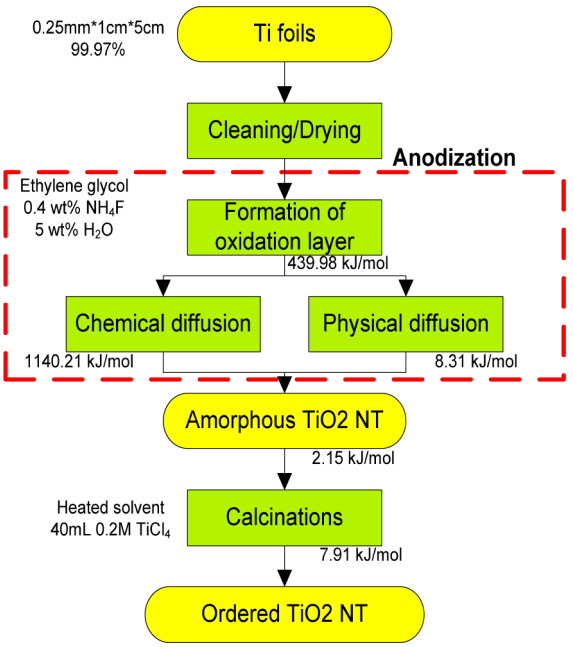

Figure 2. System boundary and Gibbs free energy associated with each process.

Model for Chemical Process in Formation of Oxidation Layer and Chemical Diffusion. The anodization process begins with an initial oxide layer formed by interaction of the surface Ti^{4+} ions with oxygen ions in the electrolyte. In the initial stages of the anodization process, field-assisted dissolution dominates the chemical dissolution due to the relatively large electric field across the thin oxide layer. Further oxide growth is controlled by field-assisted ion transport (O^{2-} and Ti^{4+} ions) through the growing oxide. The anode oxidation of titanium is shown in Figure 3.

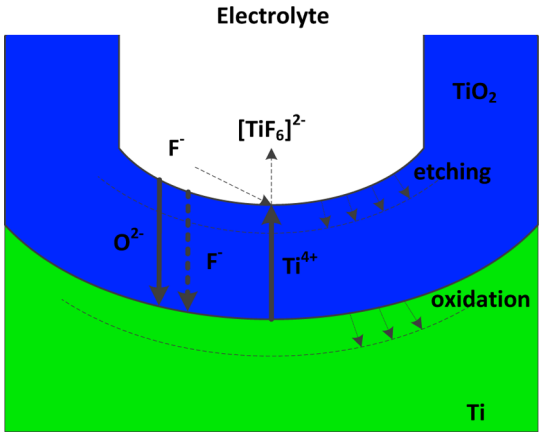

Figure 3. Schematic drawing of adonization process.[29]

Anode:

$$2H_2O \rightarrow O_2 + 4e + 4H^+ \quad \Delta G_f^0 = 6577.22 \text{ kJ}$$

$$Ti_{(s)} + O_2 \rightarrow TiO_2 \quad \Delta G_j^0 = -901.61 \text{ kj}$$

The overall anode reaction for anodic oxidation of titanium is represented as

$$Ti_{(s)} + 2H_2O_{(g)} \rightarrow TiO_{2(s)} + 4H^+ + 4e^- \quad \Delta G_f^0 = 348 \text{ kj}$$

Meanwhile, hydrogen gas is released at the cathode that causes the flotation. The electrode reaction is described as follows:

Cathode:

$$4H^+ + 4e^- \rightarrow 2H_{2(g)}$$

So the overall electrode reaction at this stage can be described as

$$Ti_{(s)} + 2H_2O \rightarrow 2H_{2(g)} + TiO_{2(s)} \quad \Delta G_f^0 = 439.98 \text{ kJ}$$

After the formation of the oxide layer, the TiO_2–Ti interface is locally activated, and the chemical and physical diffusions occur in the meantime. Small pores are formed first due to the localized dissolution of the oxide. Then, these pits are converted into bigger pores, and the pore density increases as governed by both electrochemical etching and chemical dissolution. Fluoride ions in the electrolyte have the ability to form water-soluble TiF_6^{2-}, and their small ionic radius makes them suitable to enter the growing TiO_2 lattice and to be transported through the oxide by the applied electric field. After a while, the individual pores will interfere with each other, balance the available current, and finally reach a steady state condition, which results in a growth of the self-ordered nanotube structure. The nanotubes will grow steadily when the rate of TiO_2 formation equals the rate of TiF_6^{2-} formation and dissolution. The chemical dissolution process of the oxide is described as a chemical reaction

$$TiO_{2(s)} + 6F^- + 4H^+ \rightarrow TiF_6^{2-} + 2H_2O \quad \Delta G_f^0 = 348 \text{ kJ}$$

The basic premise of electrochemical anodization is the competition between the formation of the compact TiO_2 layer and the formation/dissolution of Ti^{4+} in the nanotube TiO_2 layer.[29] After the formation of the compact TiO_2 oxide layer, Ti^{4+} ions at the metal–oxide interface will move toward the oxide–electrolyte interface under the applied electric field, as illustrated in Figure 3. On the basis of chemical thermodynamics, the overall entropy change and enthalpy change for the chemical process can be expressed in the following equations, with units in kJ/mol and kJ/mol K, respectively

$$\Delta S_{\text{Reaction}} = \sum_{\text{Products}} \gamma_i S_i - \sum_{\text{Reactants}} \gamma_i S_i \tag{1}$$

$$\Delta H^\circ_{f_{\text{Reaction}}} = \sum_{\text{Products}} \gamma_i H^\circ_{fi} - \sum_{\text{Reactants}} \gamma_i H^\circ_{fi} \tag{2}$$

The work rate for the chemical process is expressed as follows, with units in kJ/mol

$$\dot{W} = (\dot{H}_R - T_0\dot{S}_R) - (\dot{H}_P - T_0\dot{S}_P) - \left(1 - \frac{T_0}{T}\right)\dot{Q} + T_0\dot{S}_{\text{gen}} \tag{3}$$

where W is work, Q is heat, S is entropy, H is enthalpy, and γ is the stoichiometric coefficient. In this electrochemical system, the temperature change is very small and can be ignored, so the process is considered as constant temperature and pressure, which means $(1 - T_0/T)\dot{Q} = 0$. The term $\dot{S}_{\text{gen}}$ represents the entropy rate generated by irreversibilities within the process. Equation 3 provides the framework for estimating the minimum work input for this process, i.e., when irreversibilities are zero, $T_0\dot{S}_{\text{gen}} = 0$.[22] Therefore, the energy (with units in kJ/mol) equals the minimum work associated with this chemical process

$$E = W_{\text{min}} = (H_R - T_0S_R) - (H_P - T_0S_P) \tag{4}$$

dx.doi.org/10.1021/sc400304h | ACS Sustainable Chem. Eng. 2014, 2, 404–410

Model for Physical Diffusion. The current in the anodization process decreases because the diffusion of the ionic species (F^-, $[TiF_6]^{2-}$) controls the formation of the TiO_2 NTs. In this model, when the two electrodes are connected, $[TiF_6]^{2-}$ ions will be produced at the cathode, and F^- ions will be consumed at anode. On the basis of the assumption of the diffusion model by Yasuda,[30] the process can be modeled as three layers: a convection layer on the top, diffusion layer adjacent to the nanotube, and layer with the nanotube. A schematic drawing of the diffusion model for the ionic species is illustrated in Figure 4.

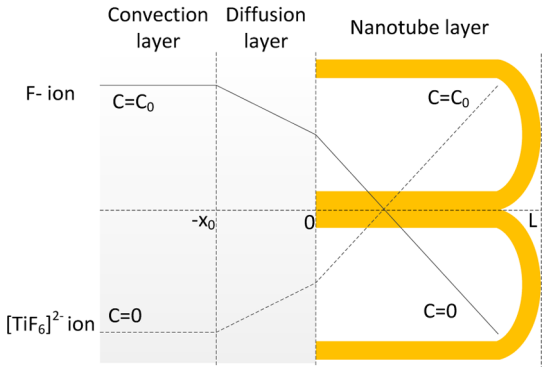

Figure 4. Schematic drawing of the diffusion model for the ionic species during anodization.[29]

Ion diffusion in the electrolyte is linear along a concentration gradient between the tube bottom and bulk electrolyte. By the definition of Fick's law of diffusion, the flux of ions (with units in mol/m^2 s) in the diffusion layer ($-x_0 \le x \le 0$) is

$$J = -D\frac{\partial C}{\partial x} \tag{5}$$

and the flux of ions in the NT layer ($0 \le x \le L$) is

$$J = -pD\frac{\partial C}{\partial x} \tag{6}$$

where J is the diffusion flux, D is the diffusion coefficient, C is the concentration, x_0 is thickness of the diffusion layer, L is length of the NT, and p is the porosity of the NT. The porosity of TiO_2 NT is calculated by the volume fraction

$$p = 1 - \frac{V_{TiO2}}{V_{Total}} \tag{7}$$

where V is the volume of component.

Because the diffusion only occurred at the bottom of the NT, the top dissolution is nearly zero. So the boundary condition (as illustrated in Figure 4) in this model is defined as follows

$$C(x \le -x_0)_F = C_0$$
$$C(x \ge L)_F = 0$$
$$C(x \ge L)_{TiF} = C_0$$
$$C(x \le -x_0)_{TiF} = 0$$

The anodic current density I (with unit in A/m^2) is described as

$$I = |nFJ| = \frac{pnFDC_0}{L + px_0} \tag{8}$$

where n is the number of electrons transported in the process, and F is the Faraday constant (96485 C mol^{-1}).

Based on the electricity principle of energy, voltage, and current, the electric energy input (with units in kJ/mol) into the physical diffusion process during time t is calculated as

$$E = U \times I \times A \times t \tag{9}$$

where U is the supplied voltage, and A is the anodized area of the Ti foil.

Model for Calcination Process. In this analysis, energy flow of a highly idealized calcination process is studied. The calcination process is modeled as an ideal steady-state open system with no heat inputs or losses, and the pressure and temperature increases are reversible. Basically, the conversion rate of the calcination process is very low; therefore, the chemical exergy change is very small when compared with the required physical exergy change and accordingly can be considered negligible. As a result, the NTs calcination process can be treated simply as raising the temperature from standard condition to reaction temperature of an air gas stream that is modeled as ideal gas in an open system. In this open system, volume is constant, so the pressure can be calculated through the classic ideal gas law. The minimum physical exergy (with units in kJ/mol) required to create the necessary conditions of the TiO_2 NT calcination process is as follows

$$b_{ph} = c_p(T - T_0) - c_pT_0 \ln\frac{T}{T_0} + T_0R \ln\frac{P}{P_0} \tag{10}$$

where b_{ph} is specific physical exergy, c_p is the heat capacity, and T_0 and P_0 are the temperature and pressure at standard conditions, respectively. On the basis of the Shomate equation, the liquid phase heat capacity can be calculated by using the average temperature T. Because this process is modeled as a reversible process ($T_0\dot{S}_{gen} = 0$), the energy of calcination process is equal to the minimum work.

$$E = b_{ph} \times m \tag{11}$$

where m is the mass of the generated TiO_2 NT.

Model for Drying Process. The drying process transfers both heat and mass, while wet air is considered as one phase homogeneous system with only two components governed by ideal gas law for fluid mixtures.[31] The energy conservation equation of drying process is presented as follows:

$$\dot{Q} - \dot{W} = \sum \dot{m}_{outlet}\left(h_{outlet} + \frac{V_{outlet}^2}{2}\right) - \sum \dot{m}_{inlet}\left(h_{inlet} + \frac{V_{inlet}^2}{2}\right) \tag{12}$$

The energy required to transfer moisture during the drying process (inside the drying box) can be quantified by the following equation

$$\dot{Q} = \dot{m}(h_{inlet} - h_{outlet}) \tag{13}$$

RESULTS

To validate the developed energy analysis model based on thermodynamics and kinetics, experiments are performed by collecting the actual experimental data during a complete electrochemical anodization process. The electrochemical anodization experiments were conducted at 30 V DC using a Ti foil as the anode, a Pt foil as the canthode, and a fluoride ion-based electrolyte. The electricity consumption in the whole process is directly monitored using a power meter. For the process parameters and materials' physicochemical properties, data from the literature are used in the analysis. A summary of the major data for this energy analysis results is presented in Table 1 below.

Among the five analyzed stages, the energy data for cleaning and drying is directly measured in the experimentation, while the data for all the other four stages in Table 1 is calculated using the developed mathematical models based on the actual experimental process parameters and data. Energy analyses for the other four stages are described afterward with more details. Detailed calculations for the required energy inputs in each of

dx.doi.org/10.1021/sc400304h | ACS Sustainable Chem. Eng. 2014, 2, 404−410

Table 1. Major Data of Energy Analysis for Electrochemical Anodization

stages	entropy (kJ/mol K)	heat (kJ/mol)	reversible work (kJ/mol)	energy (kJ/mol)
cleaning/drying		73129.13		73129.13
formation of oxide layer	−0.096	84.19	439.98	439.98
chemical diffusion	18.71	–	11406.21	11406.21
physical diffusion	–	–	–	423373.43
calcination	–	–	7.907	124189.54

the electrochemical anodization processes are included in the Supporting Information.

On the basis of the model in the Model for Chemical Process in Formation of Oxidation Layer and Chemical Diffusion section, the overall entropy change, enthalpy change and minimum work are calculated. The absolute entropy and enthalpy values for each substance in this chemical reaction is retrieved from the NIST CSTL standard reference data program in specific phase (solid, gas, and liquid) under the standard conditions (T = 25 °C, P = 1 bar). Rutile titan oxide is used in this calculation. Therefore the entropy change per mol obtained for the formation of the oxide layer is −96.42 J/mol K based on eq 1, while the enthalpy change per mol is −468.71 kJ/mol based on eq 2. The minimum work change per mol associated with the process is 439.98 kJ/mol as calculated by eq 4.

Similar to the calculation of energy requirements in the formation process of the oxide layer, the energy analysis for the chemical diffusion process is mainly built on the chemical reactions as described in the Model for Chemical Process in Formation of Oxidation Layer and Chemical Diffusion section. The process is mainly dominated by the formation and dissolution of TiF_6^{2-}. Phase rutile titan oxide and titanium fluoride is used in this calculation. The entropy change per mol obtained for the chemical diffusion process is 18705.81 J/mol K, and the minimum work rate is 11406.21 kJ/mol. The energy rate in the chemical diffusion process is 11406.21 kJ/mol.

The energy analysis of the physical diffusion process is modeled for the three layers (convection layer, diffusion layer, and nanotube layer) using eqs 5−9. In Figure 3, x_0 is determined as 10300 nm, C_0 is calculated as 2.5×10^{-5} mol/cm^3 by empirical experiment, D is set as 10^{-5}cm^2/s, and n is 4. As a result, the nDC_0 value obtained for fluoride ions in a 0.5 wt % NH_4F solution is 1.0×10^{-9} mol/cm s. In the nanotube layer, the NT diameter is 35 nm, wall thickness is 9 nm, and length is 1100 nm under 30 V experimental condition, so the porosity of TiO_2 NT in this experiment is 43.6% as calculated by eq 5. The anodic current density is 75 mA/cm^2 as calculated by eq 6. The energy requirement during the diffusion process in 2 h with a 5 cm^2 Ti anodized area is 81 kJ as calculated by eq 7. The obtained energy rate for physical diffusion process is 423373.43 kJ/mol.

The calcination process is to gradually crystallize the amorphous TiO_2 into anatase phase under moderate temperatures (200−600 °C). The crystallization process in this experiment is performed at 450 °C for 2 h, in a Thermolyne F48000 furnace with a power rating of 240 V−7.5 A−1800 W. The exergy analysis of the NTs crystallization process is conducted by raising the temperature of an air gas stream from 273 to 723 K (specific heat capacity of dry air at 400 °C is 1.068 kJ/kg K, density is 0.524 kg/m^3, and molecular mass is 28.97 g/mol).[32] The liquid phase heat capacity is calculated as 30.94 J/mol K using the Shomate equation at T = 498 K. In this system, the volume is constant, so the pressure can be calculated by classic ideal gas law. The minimum physical exergy required to create the conditions necessary to crystallize TiO_2 NT is 7.907 kJ/mol based on eq 8. The energy rate of calcinations process is 124189.54 kJ/mol, while the energy is 23.76 kJ as calculated by eq 9.

To quantify the direct energy consumption in actual TiO_2 NT production, the energy requirements in the five main stages to synthesize 1g of TiO_2 NT is illustrated in Figure 5. For the total amount of energy input into the electrochemical anodization process, the largest amount of energy input is required by the physical diffusion process, totaling 5301.05 kJ/g, accounting for 67% of the total energy requirement, while the formation of the oxide layer only requires 5.51 kJ/g of energy. This is mainly because the anodization process is dominated by the formation/dissolution of Ti^{4+} in the nanotube TiO_2 layer rather than the formation of the compact TiO_2 layer; therefore, the energy requirement for the formation of the oxide layer process is really small. When compared, the cleaning/drying and calcination processes also require significant portions of the energy input, using 11.46% and 19.65% of the total energy, respectively.

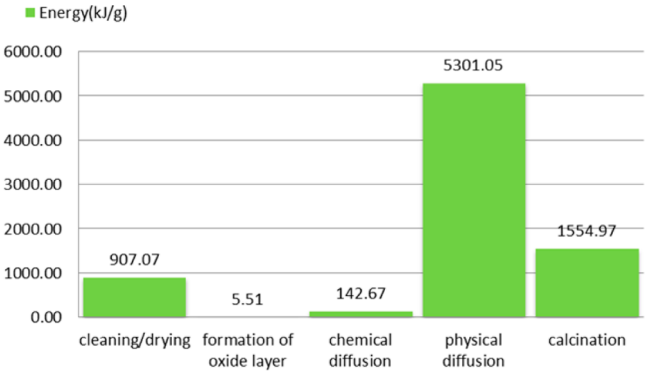

Figure 5. Direct energy consumption of synthesizing 1g of TiO_2 NT.

DISCUSSION

In general, TiO_2 nanotubes can be synthesized via different processes and pathways. The energy consumptions of these processes could be very different depending on the technology being used and the process parameters. While electrochemical anodization is a popular technique used in the TiO_2 NT synthesis, the supplied energy is important in determining both the morphologies of the TiO_2 NT structure and the sustainability performance of the technology in industrial applications. This paper aims to investigate and understand the direct energy requirements of electrochemical anodization synthesis of TiO_2 NT only.

Analyzing and understanding the direct energy requirements of the electrochemical anodization can help control the energy inputs in terms of the desired morphologies and reduce its energy consumptions in future industrial-scale applications. For the five stages analyzed during the electrochemical anodization, three processes (oxide layer formation, physical diffusion, and chemical diffusion) are inseparable in the anodization process. From the mathematical modeling process, it is shown that these

three processes operate with totally different thermodynamic/kinetic mechanisms and require different energy inputs, which are actually controlled by the supplied voltage, current, and time in the anodization process. The models and results established in this study are valuable in correlating the process energy requirement of each stage with its process parameters and will play a critical role in the future to optimize the supplied voltage, current, and time in these three processes to meet the requirements of the desired TiO_2 NT morphologies. In particular, the energy consumption in the physical diffusion process could be minimized, while meeting the requirements of oxide layer formation and chemical diffusion, in order to reduce the process energy consumption.

It must be pointed out that the models, results, and conclusions in this study are based on laboratory-scale conditions. It is highly possible that the synthesis pathways and processes could be different on the mass production of TiO_2 nanotubes in future large-scale industrial applications, but the fundamental mechanism of the electrochemical anodization of TiO_2 nanotubes should be same for this technology. It is believed that the energy models, results, and conclusions presented in this paper could provide a numerical way to calculate the direct energy consumption in the electrochemical anodization process and can be used by process designers and technology developers for future process optimization and improvement to support sustainable scale-up of the technology for large-scale industrial applications.

Though the process energy requirement is important, it is only part of the life cycle of the TiO_2 NT product. In order to understand the direct energy consumption of the electrochemical anodization process within the life cycle framework of the TiO_2 NT product, we also conducted an upstream life cycle energy analysis to quantify the energy consumptions of the materials and activities required to produce 1 g of TiO_2 NT. The life cycle energy data are retrieved from GaBi 6 professional database and literature, which are provided in Section 5 of the Supporting Information. The life cycle energy data show that the total energy consumption of raw material extractions and productions (includes Ti foil, ethylene glycol, deionized water, and ammonia fluoride) required in the experiment was approximately 3577.766 kJ. In this point, the direct energy consumption in the electrochemical anodization process only accounts for 3.4% of the total upstream energy consumption. The significant life cycle energy consumption would require further research in understanding and improving the total energy consumption of TiO_2 NT during those upstream processes.

CONCLUSION

In this paper, we report a mathematical energy modeling of the electrochemical anodization process on TiO_2 NT synthesis. To facilitate the energy modeling, the anodization process is divided into five stages including cleaning/drying, oxide layer formation, chemical diffusion, physical diffusion, and calcinations. The energy input into cleaning and drying is directly measured based on the device power and operating time. Mathematical models are developed for the other four stages based on detailed process parameters and defined boundaries. The models are finally validated through experimentation on an electrochemical anodization process at 30 V DC. The experimental data and literature data are used in the developed mathematical models to calculate the energy inputs into each process of the anodization technology. The energy analysis results of the five stages are presented and benchmarked. It demonstrates that 67% of the energy input is required by the physical diffusion process. The initial cleaning/drying and final calcination processes use 11.46% and 19.65% of the total energy, respectively. However, the oxidation layer formation process only requires 0.07% of the total energy. The developed energy models and analyses results are useful for understanding the direct energy requirements of the electrochemical anodization process and could support future scale-up of the technology for large-scale industrial applications.

ASSOCIATED CONTENT

Supporting Information

Data used in the analysis and detailed calculations for each of the anodization processes. This material is available free of charge via the Internet at http://pubs.acs.org.

AUTHOR INFORMATION

Corresponding Author

*Tel.: 414-229-5639. Fax: 414-229-6958. E-mail: cyuan@uwm.edu.

Notes

The authors declare no competing financial interest.

ACKNOWLEDGMENTS

The technical assistance and support from Dr. Zhaoyang Fan at the Nano Tech Center of Texas Tech University are gratefully acknowledged. The authors also thank the three anonymous reviewers for the constructive comments and suggestions.

REFERENCES

(1) Grimes, C.; Mor, G. *TiO_2 Nanotube Arrays: Synthesis, Properties, and Applications*; Springer: New York, 2009.

(2) Yamamoto, S.; Watabe, H.; Kanai, Y.; Imaizumi, M.; Watabe, T.; Shimosegawa, E.; Hatazawa, J. Development of a high-resolution Si-PM-based gamma camera system. *Phys. Med. Biol.* **2011**, *56* (23), 7555−7567.

(3) Shinozawa, T.; Urade, Y.; Maruyama, T.; Watabe, D. Tetranor PGDM analyses for the amyotrophic lateral sclerosis: Positive and simple diagnosis and evaluation of drug effect. *Biochem. Biophys. Res. Commun.* **2011**, *415* (4), 539−544.

(4) Kato, M.; Watabe, K.; Hamasaki, T.; Umeda, M.; Furubayashi, A.; Kinoshita, K.; Kishida, O.; Fujimoto, T.; Yamada, A.; Tsukamoto, Y.; Yamamoto, S.; Kamada, Y.; Yoshida, Y.; Kiso, S.; Tsutsui, S.; Kihara, S.; Hayashi, N.; Matsuzawa, Y. Association of low serum adiponectin levels with erosive esophagitis in men: An analysis of 2405 subjects undergoing physical check-ups. *J. Gastroenterol.* **2011**, *46* (12), 1361−1367.

(5) Asaduzzaman, M.; Kinoshita, S.; Siddique, B. S.; Asakawa, S.; Watabe, S. Multiple cis-elements in the 5 ′-flanking region of embryonic/larval fast-type of the myosin heavy chain gene of torafugu, MYHM743−2, function in the transcriptional regulation of its expression. *Gene* **2011**, *489* (1), 41−54.

(6) Tsubamoto, T.; Saneyoshi, M.; Watabe, M.; Tsogtbaatar, K.; Mainbayar, B. The entelodontid artiodactyl fauna from the Eocene Ergilin Dzo Formation of Mongolia with comments on Brachyhyops and the Khoer Dzan locality. *Paleontol. Res.* **2011**, *15* (4), 258−268.

(7) Watabe, Y.; Noguchi, T. Site-investigation and geotechnical design of D-runway construction in Tokyo Haneda Airport. *Soils Found.* **2011**, *51* (6), 1003−1018.

(8) Tahara, M.; Sakai, H.; Nishikomori, R.; Yasumi, T.; Heike, T.; Nagata, I.; Inui, A.; Fujisawa, T.; Shigematsu, Y.; Nishijima, K.; Kuwakado, K.; Watabe, S.; Kameyama, J. Patient with neonatal-onset chronic hepatitis presenting with mevalonate kinase deficiency with a novel MVK gene mutation. *Mod. Rheumatol.* **2011**, *21* (6), 641−645.

(9) Cao, H. L.; Wang, X. L.; Gao, J. J.; Prigent, S. R.; Watabe, H.; Zhang, Y. P.; Chen, H. W. Phylogeny of the African and Asian Phortica (Drosophilidae) deduced from nuclear and mitochondrial DNA sequences. *Mol. Phylogenet. Evol.* **2011**, *61* (3), 677−685.
(10) Inoue, H.; Takenaga, M.; Ohta, Y.; Tomioka, M.; Watabe, Y. I.; Aihara, M.; Kumagai, N. Improvement of hind-limb paralysis following traumatic spinal cord injury in rats by grafting normal human keratinocytes: New cell-therapy strategy for nerve regeneration. *J. Artif. Organs* **2011**, *14* (4), 375−380.
(11) Kojima, T.; Watabe, T.; Nakamura, T.; Ichikawa, K.; Satoh, Y. Effects of preoperative punctal plug treatment on visual function and wound healing in laser epithelial keratomileusis. *J. Refract. Surg.* **2011**, *27* (12), 894−898.
(12) Kobayashi, S.; Hamasaki, N.; Suzuki, M.; Kimura, M.; Shirai, H.; Hanabusa, K. Preparation of helical transition-metal oxide tubes using organogelators as structure-directing agents. *J. Am. Chem. Soc.* **2002**, *124* (23), 6550−6551.
(13) Gao, X.; Chen, J.; Yuan, C. Enhancing the performance of free-standing TiO_2 nanotube arrays based dye-sensitized solar cells via ultraprecise control of the nanotube wall thickness. *J. Power Sources* **2013**, *240* (0), 503−509.
(14) Tian, Z. R.; Voigt, J. A.; Liu, J.; McKenzie, B.; Xu, H. Large oriented arrays and continuous films of TiO_2-based nanotubes. *J. Am. Chem. Soc.* **2003**, *125* (41), 12384−12385.
(15) Bavykin, D. V.; Friedrich, J. M.; Walsh, F. C. Protonated titanates and TiO_2 nanostructured materials: Synthesis, properties, and applications. *Adv. Mater.* **2006**, *18* (21), 2807−2824.
(16) Yao, B. D.; Chan, Y. F.; Zhang, X. Y.; Zhang, W. F.; Yang, Z. Y.; Wang, N. Formation mechanism of TiO_2 nanotubes. *Appl. Phys. Lett.* **2003**, *82* (2), 281−283.
(17) Ji, Y.; Zhang, H.; Ma, X.; Xu, J.; Yang, D. Single-crystalline SnS_2 nano-belts fabricated by a novel hydrothermal method. *J. Phys.: Condens. Matter* **2003**, *15* (44), L661.
(18) Pang, S. C.; Chin, S. F.; Ling, C. Y. Controlled synthesis of manganese dioxide nanostructures via a facile hydrothermal route. *J. Nanomater.* **2012**, *2012*.
(19) Chen, X.; Mao, S. S. Titanium dioxide nanomaterials: Synthesis, properties, modifications, and applications. *Chem. Rev.* **2007**, *107* (7), 2891−2959.
(20) Yuan, C.; Dornfeld, D. A schematic method for sustainable material selection of toxic chemcials in design and manufacturing. *J. Mech. Des.* **2010**, *132* (9), 091014.
(21) Alivov, Y.; Pandikunta, M.; Nikishin, S.; Fan, Z. Y. The anodization voltage influence on the properties of TiO_2 nanotubes grown by electrochemical oxidation. *Nanotechnology* **2009**, *20* (22), 225602.
(22) Gutowski, T. G.; Branham, M. S.; Dahmus, J. B.; Jones, A. I.; Thiriez, A.; Sekulic, D. P. Thermodynamic analysis of resources used in manufacturing processes. *Environ. Sci. Technol.* **2009**, *43* (5), 1584−1590.
(23) Grubb, G. F.; Bakshi, B. R. Appreciating the role of thermodynamics in LCA improvement analysis via an application to titanium dioxide nanoparticles. *Environ. Sci. Technol.* **2011**, *45* (7), 3054−3061.
(24) Zhu, Z. C.; Chen, H. L.; Chang, L. F.; Li, B. Dynamic model of ion and water transport in ionic polymer-metal composites. *AIP Adv.* **2011**, *1* (4), 040702.
(25) Li, B.; Lee, C. NEMS diaphragm sensors integrated with triple-nano-ring resonator. *Sens. Actuators, A* **2011**, *172* (1), 61−68.
(26) Gottschalk, F.; Scholz, R. W.; Nowack, B. Probabilistic material flow modeling for assessing the environmental exposure to compounds: Methodology and an application to engineered nano-TiO_2 particles. *Environ. Modell. Software* **2010**, *25* (3), 320−332.
(27) Grubb, G. F.; Bakshi, B. R. Life cycle of titanium dioxide nanoparticle production impact of emissions and use of resources. *J. Ind. Ecol.* **2011**, *15* (1), 81−95.
(28) Theis, T. L.; Bakshi, B. R.; Durham, D.; Fthenakis, V. M.; Gutowski, T. G.; Isaacs, J. A.; Seager, T.; Wiesner, M. R. A life cycle framework for the investigation of environmentally benign nanoparticles and products. *Phys Status Solidi-R* **2011**, *5* (9), 312−317.
(29) Macak, J. M.; Tsuchiya, H.; Ghicov, A.; Yasuda, K.; Hahn, R.; Bauer, S.; Schmuki, P. TiO_2 nanotubes: Self-organized electrochemical formation, properties and applications. *Curr. Opin. Solid State Mater. Sci.* **2007**, *11* (1−2), 3−18.
(30) Li, B. Q.; Abran, M.; Matteau-Pelletier, C.; Rouleau, L.; Lam, T.; Sharma, R.; Rheaume, E.; Kakkar, A.; Tardif, J. C.; Lesage, F. Low-cost three-dimensional imaging system combining fluorescence and ultrasound. *J. Biomed. Opt.* **2011**, *16* (12), 126010.
(31) Boulemtafes-Boukadoum, A.; Benzaoui, A. Energy and exergy analysis of solar drying process of mint. *Energy Proc.* **2011**, *6* (0), 583−591.
(32) Air Properties. The Engineering Toolbox. http://www.engineeringtoolbox.com/air-properties-d_156.html (accessed February 26, 2013).